Non-enzymatic Determination of Glucose in Artificial Urine Using 3D-μPADs through Silver Nanoparticles Formation

Ahmad Luthfi Fahmi, Kamila Rohadatul 'Aisy, Ika Oktavia Wulandari, Hermin Sulistyarti, and Akhmad Sabarudin*

Department of Chemistry, Faculty of Science, Universitas Brawijaya, Jl. Veteran No. 12-16, Malang 65145, Indonesia

* ***Corresponding author:***

email: sabarjpn@ub.ac.id

Received: April 23, 2024
Accepted: July 8, 2024

DOI: 10.22146/ijc.95588

Abstract: *Patients with diabetes often experience blood glucose fluctuations, making monitoring crucial. Traditional blood sampling methods pose risks of infection and pain. An alternative non-invasive approach using urine tests has been explored. Recent studies highlight microfluidic paper-based analytical devices (μPADs) as convenient, simple, and easily fabricated tools for non-invasive glucose measurement. This study aims to develop a concept of measuring glucose in artificial urine using 3D-μPADs in a non-enzymatic manner by utilizing glucose as a reducing agent for silver nanoparticle (AgNPs) formation. Embedding three-dimensional connectors in μPADs links the sample and detection zones to limit reagent mixing and improve glucose detection resolution. The optimal conditions were NaOH 10 M, starch 1%, and $AgNO_3$ 30 mM, with sample and detection zone volumes of 10 and 9 μL, respectively. The fifth reaction sequence involved $AgNO_3$ in the detection zone and a solution of glucose, NaOH, and starch in the sample zone at 1:1:1 volume ratio. The reagent drying time was 15 min, with immobilization once and reaction time of 9 min. The method showed excellent linearity (R^2 = 0.9905), precision (%RSD = 4.27%), accuracy (77.32–92.58%), and limit of detection (11.11 mg/dL).*

Keywords: *glucose; ImageJ; non-invasive; paper-based devices; silver nanoparticle*

■ INTRODUCTION

Diabetes mellitus is a symptom of hyperglycemia, which is characterized by an increase in glucose levels in the body's metabolic system. Untreated patients can cause serious complications like stroke, heart disease, cataracts, kidney problems, and other serious effects [1-3]. Type II diabetes mellitus is particularly common and is often associated with decreased insulin activity. Insulin plays a crucial role as the hormone responsible for reducing glucose levels in the body [4-6]. Genetic factors, metabolism, and an unhealthy environment are key contributors to this decreased insulin activity. High glucose levels in the body can make it difficult for pancreatic beta cells to control it, thus, resulting in insulin release that is not proportional to the glucose intake [7]. Such conditions will trigger persistent hyperglycemia, which causes symptoms of diabetes mellitus to appear.

Glucose contributes to supporting the supply of adenosine triphosphate (ATP) production, allowing the body to function normally [4]. Due to the importance of glucose for the body, it needs to be fully distributed throughout the body via the bloodstream. Blood regulation is related to kidney filtration, so fluctuations in blood glucose also affect the glucose levels in urine. In acute conditions, the kidney glomerulus can swell, causing urine to contain high glucose level (glycosuria). This swelling usually occurs due to problems with glucose reabsorption in the sodium-glucose cotransporter type II [8-10]. Normal urine contains glucose below 15 mg/dL, while the urine of diabetic patients contains glucose in a range of 50–100 mg/dL [11-12].

The phenomenon would provide benefits if the approach through silver nanoparticle (AgNPs) synthesis were applied as a non-invasive early detection system for diagnosing diabetes. Several literatures indicate that AgNPs can be synthesized through the glucose reduction process. Recent studies have identified glucose

as an effective reducing agent for Ag^+ when oxidized by a base like NaOH. This oxidation process transforms glucose into a carbanion that reduces Ag^+ ions to AgNPs. However, controlling the size and stability of AgNPs presents a challenge. Uncontrolled aggregation can occur when Ag^0 nanoparticles interact with remaining Ag^+. To address this issue, capping agents are employed during synthesis. Starch, a biocompatible and readily available material, has emerged as a promising capping agent due to the presence of glycosidic bonds in its amylose and amylopectin components [13-16]. If this AgNP synthesis is applied as a measurement, it can provide an alternative enzyme-based glucose measurement that is sensitive to pH and temperature [17].

Recent research indicates that microfluidic paper-based analytical devices (μPADs) have significant potential for application in glucose detection based on AgNPs. This is attributed to μPADs meeting the affordable, sensitive, specific, user-friendly, rapid and robust, equipment-free, and deliverable to end-users (ASSURED) criteria as defined by the WHO. These criteria enable μPADs to serve as diagnostic tools that can be operated with high portability, allowing many individuals to monitor their blood glucose levels without being hindered by limited access to healthcare [18-19]. Among the two commonly used μPADs methods, distance-based testing offers greater convenience compared to colorimetry, as it does not require additional external instruments. This method measured biomarker levels based on the difference in reaction lengths. The difference in reaction lengths facilitates easier observation compared to colorimetry, which relies primarily on visual color sensitivity [20]. However, conventional distance-based methods have limitations due to uncontrolled mixing of reagents between the detection and sample zones caused by capillary action. To address this issue, Al-Jaf and Omer [21] introduced the concept of a 3D-connector, which effectively limits the sample and detection zones and prevents capillary flow from affecting uncontrolled reagent dispersion. This concept serves as the basis for the development of 3D-μPADs in this research.

Although the integration of AgNPs synthesis and 3D-μPADs offers a promising solution for portable glucose measurement, challenges arise in mass production using conventional μPADs printing methods. To address this issue, this study proposes the use of wax printing. This method provides advantages due to its computerization, which enables precise replication of designs. Therefore, the aim of this research is to develop a combination of AgNPs synthesis, 3D-μPADs concept, and mass production through wax printing to have the potential to develop a robust, portable, and easily accessible glucose measurement system in various regions with limited healthcare access [22]. The advancement of glucose measurement methods based on AgNPs using 3D-μPADs can provide convenience for many individuals to monitor their glucose levels without the need for invasive testing and enzyme-based methods, which have been historically limited by weaknesses.

■ EXPERIMENTAL SECTION

Materials

The materials utilized in this study include Whatman No. 1 chromatography paper sourced from Cytiva (China), D-(+)-glucose anhydrous, soluble starch, silver nitrate, sodium hydroxide, citric acid (≥ 98%), and sodium chloride (≥ 99.0%) obtained from Merck (Germany). Additionally, sodium bicarbonate (99.5–100.5%), uric acid (≥ 99%), sodium sulfate decahydrate (≥ 99.0%), potassium dihydrogen phosphate (≥ 99.0%), dipotassium hydrogen phosphate (≥ 99.0%), ammonium chloride (≥ 99.5%), lactic acid (≥ 98%), calcium chloride dihydrate (≥ 99.0%), magnesium sulfate heptahydrate (≥ 99.0%), and urea were procured from Sigma Aldrich (United States). Distilled water served as the solvent for the experiments.

Instrumentation

The ColorQube 850 DN Solid Ink Color printer was utilized to produce 3D-μPADs. Microwave heating was employed to facilitate wax penetration into the paper, while the design of the 3D-μPADs was crafted using CorelDraw Portable 2019 software. ImageJ 1.53t software was then utilized to assess both the slope and propagation (distance) reaction length. The images were

captured using a 25-megapixel cell phone camera inside the Photo box PULUZ Mini Studio, ensuring stable LED lighting.

Procedure

3D-μPADs fabrication

The design of the μPADs was created using CorelDraw 2019 software and printed on Whatman No. 1 paper. The 3D-μPADs design was made with ink thickness dimensions as shown in Fig. 1. The overall design dimensions were 61.56 × 14.20 mm, with the sizes of several other zones such as the detection zone measuring 35 × 2 mm, the sample zone measuring 4.68 × 2.8 mm, and the 3D-connector measuring 7.83 × 2.8 mm. The fabrication of 3D-μPADs was carried out using the wax printing method with a Xerox ColorQube 8580 DN solid ink printer. After printing, the paper was heated in the oven at 120 °C for 4 min to allow the ink to penetrate the pores and form a hydrophobic barrier. The fabrication of this hydrophobic barrier aims to control the occurrence of specific reactions on the targeted surface of the paper substrate, as well as prevent fluid leakage to undesired areas of the substrate. Subsequently, the wax-treated paper was cut along the design boundaries using a paper cutter or scissors. Once cut, the 3D-μPADs design was ready for use. The complete fabrication process is illustrated in Fig. 1.

Analysis and in-situ *synthesis AgNPs on 3D-μPADs*

The synthesis of AgNPs in situ on 3D-μPADs can be conducted following the procedure illustrated in Fig. 2. Silver nitrate with a concentration of 30 mM is applied as elongated droplets to the detection zone from bottom to top, totaling 9 μL. After the application process, the droplets are dried for 15 min at a constant temperature of 25 °C. Subsequently, the medium is folded at the 3D-connector, taped, and clamped on both sides using acrylic. A solution containing 100 mg/dL standard glucose, 10 M NaOH, and 1% starch in a volume ratio of 1:1:1 was dispensed onto the sample zone in an amount of 10 μL. The optimal sample and detection zone volumes were determined based on previous optimization efforts.

These optimal conditions were selected based on ImageJ analysis of the highest blue intensity slope. Within the 3D-μPADs detection zone, a chemical reaction takes place. Glucose is oxidized by NaOH to form a carbanion, which reduces Ag^{+} from silver nitrate

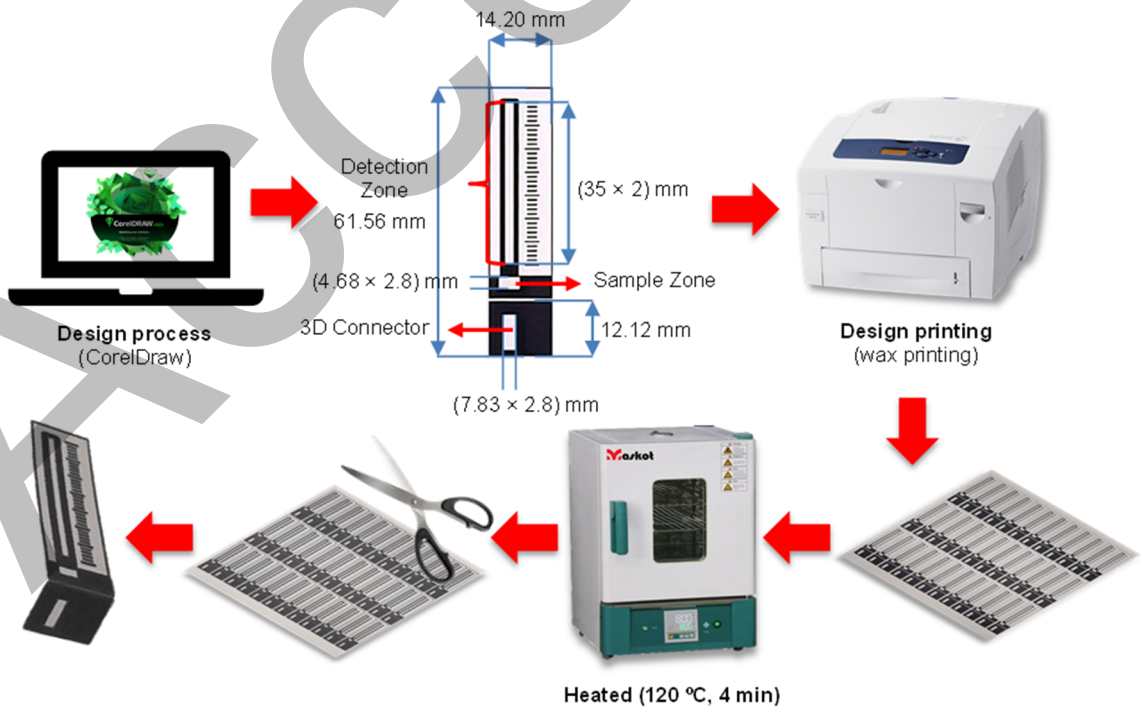

Fig 1. Scheme for 3D-μPADs fabrication

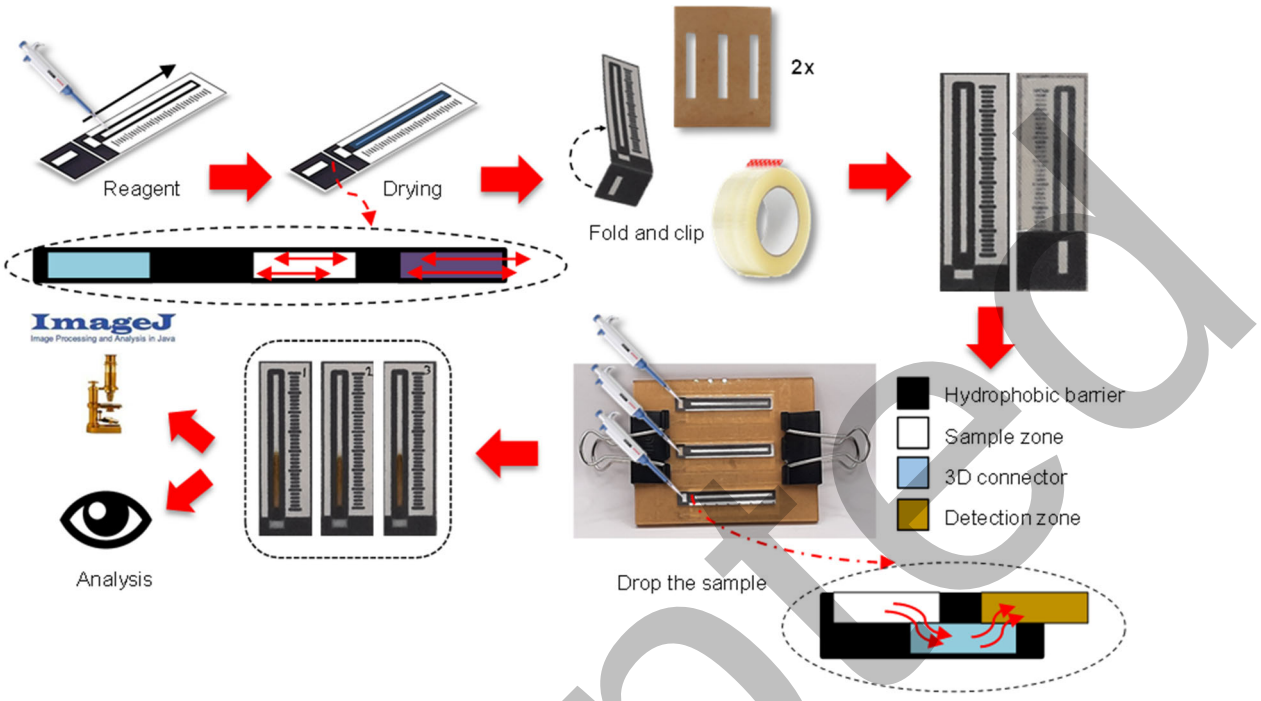

Fig 2. Glucose measurement via *in-situ* AgNPs formation on 3D-μPADs

to chargeless silver ions (Ag^0) or AgNPs. To prevent the agglomeration of AgNPs with other unreduced Ag^+, starch is employed as a capping agent due to its glycosidic bonds. After dispensing, the mixture of 100 mg/dL standard glucose solution that has been oxidized by a base was allowed to form a reaction propagation for 9 min.

Observation data are analyzed using naked eye observation and ImageJ. In ImageJ analysis, optimum conditions can be determined by considering each observed variation's slope value (y/x). The calculation of the slope value can be done according to the procedure in Fig. 3. The reaction distance can be measured using the 'straight' tool. Next, the red, green, blue (RGB) spectrum readings scale can be set through the following menu sequence: 'analyze', 'set scale', 'known distance = 35 mm', 'unit of length = mm', and check 'global'. Raw data can be extracted to Ms. Excel via the 'list' menu. Then, the determination of coordinate points can be used to establish the slope value. High slope values (y/x) indicate clear color boundaries and are suitable to be used as a measurement method in 3D-μPADs. The blue color intensity is chosen due to its complementary nature to the AgNPs color. Additionally, the slope value of the blue color intensity is greater than that of the other color intensities in ImageJ analysis.

Method validation

Optimal conditions derived from six parameters including sequence of reaction methods, sample and detection zone volumes, reagent concentration, reagent drying time, reagent immobilization, and reaction time are validated for method validation. Method validation encompasses linearity, precision, accuracy, and limit of detection (LOD). The optimized parameters are then applied to method validation. Linearity assessment is performed using artificial urine (composition detailed in Table S1 [23]) with standard glucose analyte concentrations of 0, 5, 15, 25, 50, 75, and 100 mg/dL. Precision is evaluated by measuring the standard glucose analyte concentration in artificial urine six times and assessing measurement consistency using relative standard deviation (%RSD). Conversely, accuracy is determined by measuring glucose analyte concentrations of 5, 15, 25, 50, 75, and 100 mg/dL in artificial urine and comparing them to the actual standard glucose analyte at equivalent concentrations. In addition to the three method validations mentioned,

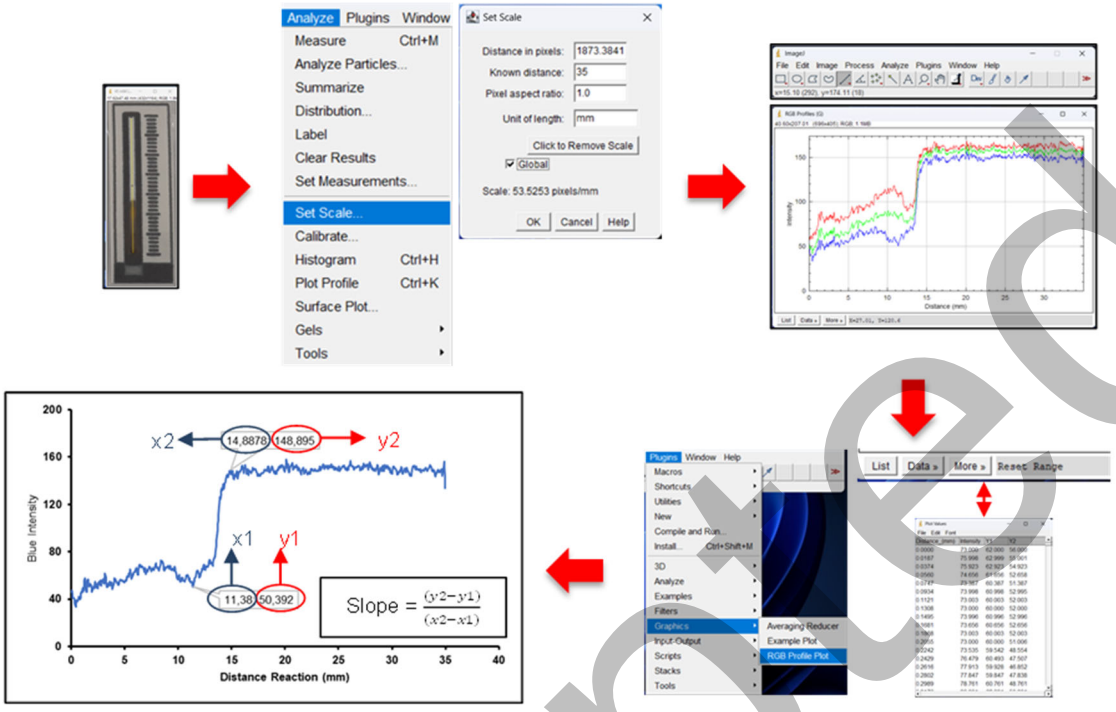

Fig 3. Analysis of reaction distances using ImageJ measurements

the capability of 3D-μPADs was also evaluated to determine the LOD for standard glucose analyte concentrations. This LOD determination was conducted through three replicate measurements of the analyte for each standard.

■ RESULTS AND DISCUSSION

Effect Penetrating Wax on 3D-μPADs

Changes in wax heating during penetration significantly impact the formation of hydrophobic barriers within the device. Notably, the detection zone, sample zone, and 3D-connector experience a narrowing effect. This narrowing phenomenon was clearly observed during zone measurements using CorelDraw 2019 software, as illustrated in Fig. 4. Before the design is heated, the ink thickness of the design shows the same dimensions as when the design size was created. The dimensions for the detection zone, sample zone, and 3D-connector were 35×2, 4.68×2.8, and 7.83×2.8 mm, respectively. The hydrophobic barrier region in the 3D-μPADs expands upon heating with the oven. Specifically, the detection zone expands by 0.902×0.283 mm, the sample zone by 0.520×0.402 mm, and the 3D-connector

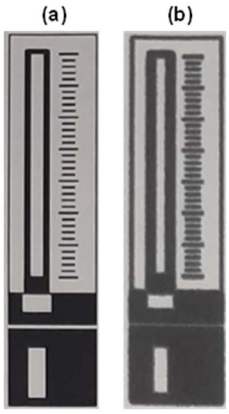

Fig 4. (a) Before and (b) after wax penetration through heating on paper substrate

by 0.783×0.482 mm. Even though changes still occur, precise mold shapes between designs can still be achieved to improve the accuracy of glucose measurement. Smaller design scale differences can minimize measurement errors. The measurement scale observations from the images are detailed in Table S2.

Impact of Glucose on AgNPs Formation in 3D-μPADs

Glucose as the target analyte affects the formation

of AgNPs. The effect of glucose levels can be seen in Fig. 5. Observations show that the higher the glucose analyte level, the greater its influence on nanoparticles' color and propagation length in the detection zone. The phenomenon can be explained through the reaction mechanism shown in Fig. 6. The glucose structure has an aldehyde group that is easily oxidized. The oxygen atom in the aldehyde group tends to show its electronegativity, which triggers the carbon atom to be more positively charged. This electron-deficient condition of the carbon atom allows nucleophilic addition to occur in an alkaline medium. This nucleophilic addition affects the carboxyl group of glucose, which can be converted into a carbanion. The carbanion group then reduces Ag^+ to Ag^0 [24-25].

The process of glucose reducing Ag^+ in an alkaline medium tends to produce nanoparticle agglomeration. This emphasizes the need for a substance that can control nanoparticle dispersion. Polysaccharides like starch emerge as one of the readily available biodegradable materials that can act as stabilizing agents [26-27]. Starch has superior stabilization ability compared to materials like D-glucose. This is due to the starch polymer having amylose and amylopectin chains. The arrangement of α-glycosidic bonds in these chains enhances the effectiveness of stabilizing AgNP distribution, as depicted in Fig. 7. The Ag_2^+ ion is formed from the Ag^+ ion and Ag^0. The dimerization of the Ag_2^+ ion will form Ag_4^{2+}. One Ag_4^{2+} ion attaches to the α-glycosidic bond and the aldehyde group on the glucose unit in the polysaccharide chain of starch. This indicates that each glucose unit and glycosidic bond can accommodate nanoparticles (Ag^0) [28-29]. This capability allows for reducing AgNPs aggregation by controlling starch concentration. Proper adjustment of starch concentration would significantly contribute to ensuring color uniformity and regulating propagation length in μPADs.

Besides agglomeration, the presence of intermediate ions in artificial urine also affects the reduction process of AgNPs. The composition of artificial urine containing acidic or salt substances can influence the pH of glucose oxidation by base, significantly affecting the kinetics of the reduction reaction and the final size of AgNPs [30]. Some components of artificial urine even have the potential to interact with NaOH, thereby affecting the overall reaction conditions. However, these conditions can be overcome by optimizing the concentration parameters of the reagents. At low concentrations, the reaction propagation experiences disturbance indicated by the fading of the reaction distance. This serves as evidence that the complexity of artificial urine components also influences the reduction process of AgNPs. Therefore, the determination of reagent concentrations is generally carried out at high concentrations or even approaching saturation to address disturbances caused by some components in artificial urine.

Determination of Reaction Sequence for Glucose Detection

The correct synthesis sequence can affect the optimal formation of nanoparticles in the detection zone. The observation results from the selection of five

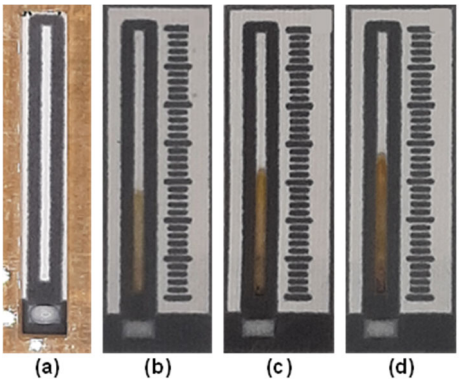

Fig 5. Sample before measurement on (a) 3D-μPADs, (b) blank sample, (c) 50 mg/dL glucose and (d) 100 mg/dL glucose in artificial urine samples

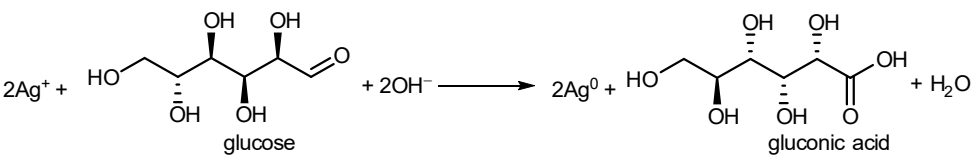

Fig 6. Mechanism of reducing Ag^+ by glucose in alkaline medium to form AgNPs

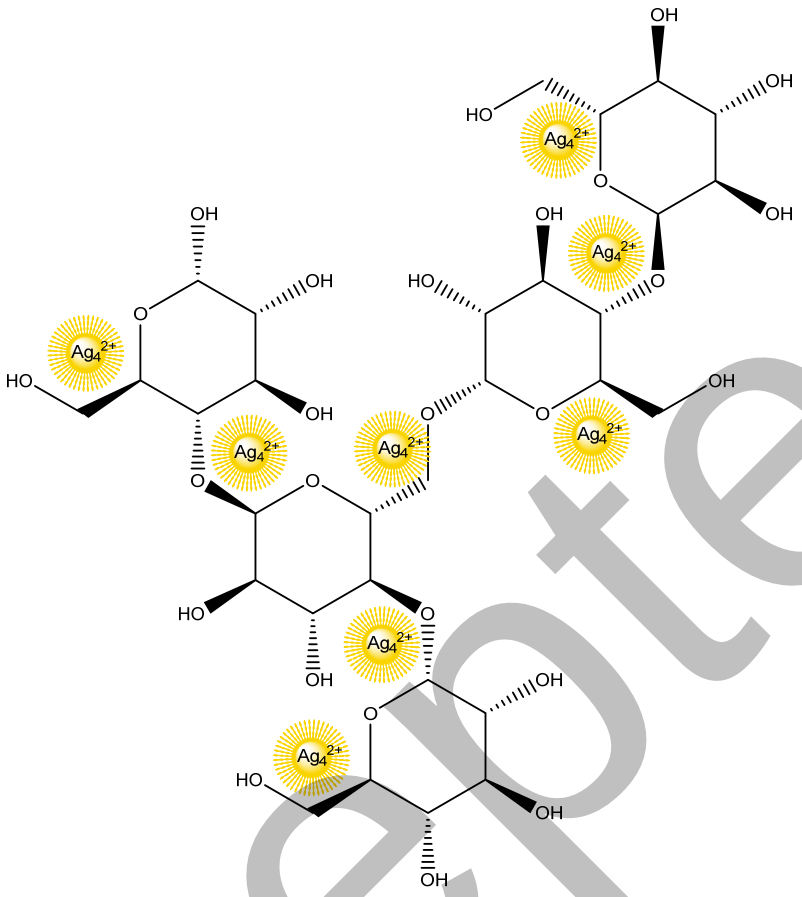

Fig 7. Illustration of AgNPs distribution on the glycosidic bond of polysaccharide capping agent starch

reaction sequence methods are presented in Table 1 and Fig. S1. The reaction sequence in Table 1 is determined based on Fig. 2. The reaction sequence begins with the dropping and drying of reagents in the detection zone. Following the process flow in Fig. 2, the process is finalized by dropping the sample solution according to Table 1 on the sample zone. The difference between the first and second methods lies in the order of dropping. In the first method, glucose in artificial urine and NaOH are mixed in a volume ratio of 1:1 and then dropped on the sample zone. In the second method, the solutions are dropped separately. The first drop is glucose in artificial urine, followed by the second drop of NaOH. Three synthesis sequence methods for AgNPs successfully demonstrate color changes. Three methods were re-selected to obtain clear boundaries in measurement observation. A comparison of the three methods is shown in Fig. 8. Analysis of the blue intensity slope shows that the fifth synthesis method is more effective than the other two methods. This phenomenon shows

Table 1. Sequence method of synthesizing AgNPs on 3D-μPADs for glucose detection

Sequence study	Sample zone	Detection zone	Results
Method 1	Glucose + NaOH	$AgNO_3$ + starch	Colored*
Method 2	Glucose + NaOH	$AgNO_3$ + starch	Colored*
Method 3	Glucose + $AgNO_3$	NaOH + starch	Colorless
Method 4	Glucose + starch + $AgNO_3$	NaOH	Colorless
Method 5	Glucose + NaOH + starch	$AgNO_3$	Colored*

*Brown-yellowish

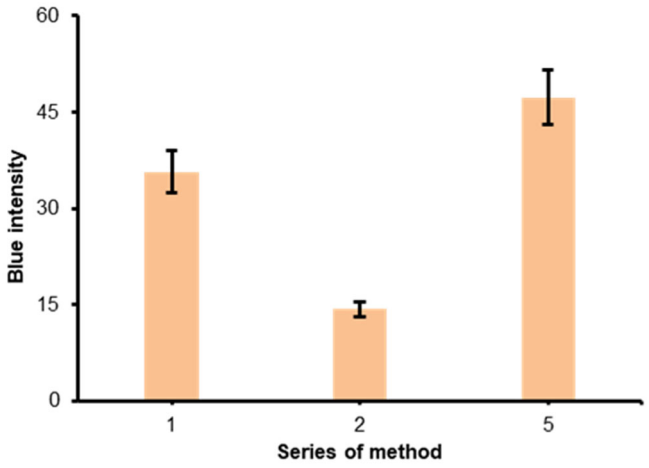

Fig 8. Selection of three reaction sequence methods 1st (M1), 2nd (M2), and 3rd (M5). See Table 1 for the reaction sequences

that the order of AgNPs synthesis affect the formation of optimal color boundaries in the detection zone. An inappropriate sequence of synthesis methods can eliminate the color reaction distance in the detection zone, such as in the third and fourth methods. This condition confirms that without being oxidized by alkaline media, glucose cannot reduce Ag^+ ions [13-16]. The phenomenon is reinforced by Fig. S2, which illustrates the condition of glucose without alkaline media. Additionally, the distribution control of AgNPs can be well observed in the fifth method.

Optimization Sample and Detection Zone Volumes on 3D-µPADs

The use of a suitable sample and reagent volume will produce clear color boundaries for measurement observation. This effect needs to be considered in the development of new measurement methods. The initial determination was conducted on the sample zone volume using a dye propagation test, as illustrated in Fig. S3. The results of this test are used to determine the capacity range for the sample zone volume in the detection zone. This method is beneficial for mapping the fluid capacity that is not obstructed by hydrophobic barriers, with the mapping based on the diffusion process of dye in the pores of the paper substrate [31]. The analysis of the blue intensity slope was performed on the range of dye testing, according to Fig. 9(a). The analysis for determining the sample zone volume was conducted within the range of 8 to 13 µL. This analysis was based on the reaction distance that resulted in the highest blue intensity slope. The analysis found that the optimal sample zone volume is 10 µL. The blue intensity slope analysis revealed an initial increase followed by a subsequent decrease beyond this volume. Similarly, the detection zone volume was determined while maintaining the sample zone volume at 10 µL, as depicted in Fig. 9(b). The optimal volume of the detection zone using ImageJ was also determined within the range of 8 to 13 µL. The highest blue intensity slope indicated the most distinct and optimal color boundary, which was easily observable with the naked eye as well as using ImageJ. The analysis results show that the optimal volume for the detection zone is 9 µL. The graph shows that after reaching this volume, there is an increase followed by a decrease.

Effect of Reagent Concentration

The concentration of reagents plays a crucial role in controlling color propagation and nanoparticle size

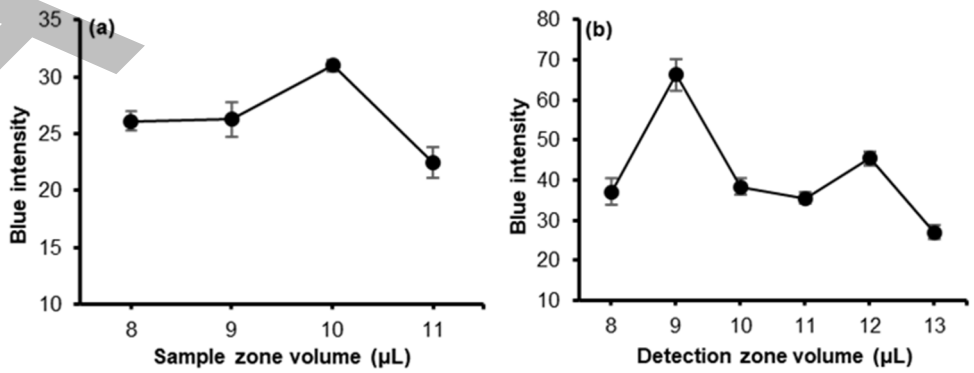

Fig 9. Optimizing volumes of (a) sample zone and (b) detection zone in 3D-µPADs

distribution on μPADs. This influence was investigated by observing key reagents such as NaOH, starch, and $AgNO_3$ while setting several control variables. Reagent concentrations were manipulated as independent variables across a range of silver nitrate concentrations, spanning from 15 to 45 mM. Color boundary analysis indicates that increasing the concentration of $AgNO_3$ precursor influences the quantity and size control of synthesized AgNPs, as shown in Fig. 10(a). The optimal size of AgNPs is around 60–90 nm. However, this study does not specifically address the issue of size. Instead, this study examines the formation of AgNPs from reducing agents with different analyte concentrations, ensuring that the reaction length obtained reflects the amount of AgNPs reduced from glucose. This research focuses mainly on the formation of yellow-brown color propagation with the most distinct color boundaries while still reflecting the characteristics of AgNPs to facilitate observation by the naked eye and ImageJ [32]. ImageJ analysis of each silver nitrate concentration reveals an increase in the intensity of the blue spectrum slope up to 30 mM, followed by a decrease at 45 mM, as depicted in Fig. 10(a). Continuously increasing the concentration of silver nitrate does not lead to the formation of AgNPs under optimal conditions. As illustrated in Fig. 10(a), increasing the silver nitrate concentration leads to the formation of visible AgNP aggregates with dark reaction diffusion boundaries at a concentration of 45 mM. These aggregates and dark boundaries induce a downward trend in the slope of the

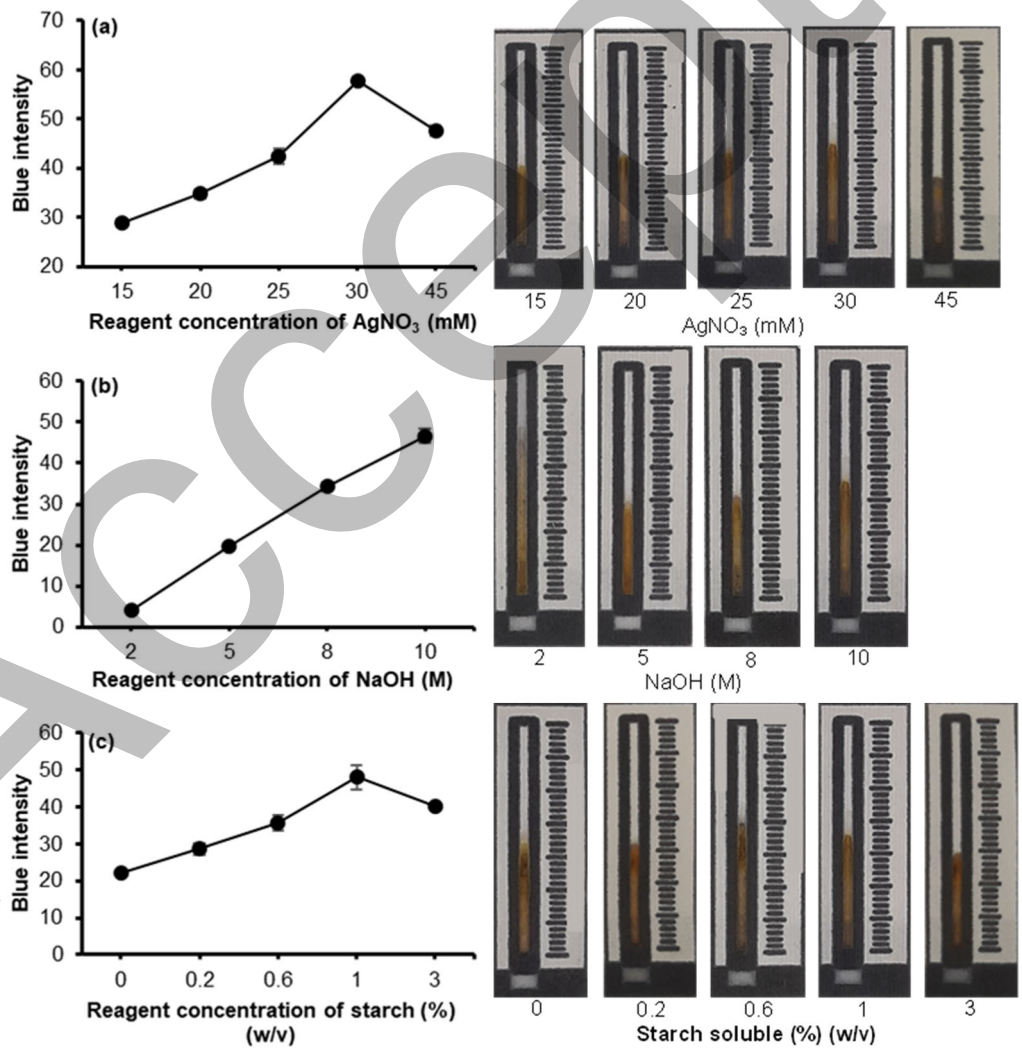

Fig 10. Effect of (a) $AgNO_3$, (b) NaOH, and (c) starch concentrations for the AgNPs formation on 3D-μPADs

blue intensity, which signifies the sharpness of the color change, starting at a concentration of 45 mM. This suggests that the optimal glucose concentration of 100 mg/dL can effectively reduce silver nitrate up to 30 mM, with other variables such as 10 M NaOH and 1% starch held constant. The saturation condition of 100 mg/dL glucose is indicated by the darkening color propagation accompanied by a decrease in the blue intensity slope.

The increased NaOH concentration significantly influences the 100 mg/dL glucose reduction process. The concentration of NaOH was varied from 2 to 10 M while maintaining optimal conditions, as depicted in Fig. 10(b). The analysis of the blue intensity slope shows that the intensity increases gradually until the NaOH concentration reaches 10 M, approaching its solubility limit, as shown in Fig. 10(b). The saturation point of NaOH at 0 °C is 42 g per 100 mL, while preparing a 10 M NaOH solution requires 40 g per 100 mL [33]. This close proximity in dissolved mass necessitates halting the optimization process due to the onset of NaOH saturation. Forcing the NaOH concentration higher would likely result in a flat graph trend due to saturation, rendering further optimization ineffective. According to Fig. 10(b), increasing NaOH shows optimal results when approaching the saturation point of 10 M. At this point, the reaction distance boundary becomes sharper. It can be observed clearly by both the naked eye and through ImageJ. This condition shows that the ability of NaOH to reduce 100 mg/dL glucose is only up to that concentration. This phenomenon indicates that optimal AgNP formation requires attention to the solubility of NaOH in oxidizing glucose.

Starch optimization was carried out at various concentrations ranging from 0 to 3% to evaluate the effectiveness of the stabilizing agent in reducing the agglomeration of 100 mg/dL glucose. The results showed that increasing the starch concentration affected the color uniformity, as shown in Fig. 10(c). Analysis of the blue intensity slope showed that the increase in distribution effectiveness was obtained up to 1%, but a decrease was observed outside this concentration, as shown in Fig. 10(c). This finding suggests that 1% starch optimally facilitates the distribution of AgNPs in the 100 mg/dL glucose reduction process. Fig. 10(c) shows that an excessive increase in starch concentration can lead to the formation of uncontrolled agglomerates, indicated by a darkening of the reaction propagation boundary in the detection zone. This suggests that control over starch concentration has an optimal limit for regulating agglomerate formation. If the starch concentration is not effectively controlled, such as at 3%, agglomerates may reform, leading to a decline in the trend of the blue intensity slope signal graph. Moreover, concentrations exceeding 1% did not improve aldehyde groups' ability or α-glycosidic bonds' ability to reduce AgNPs agglomeration.

Effect of Reagent Drying Time

This observation focused on the influence of drying time maintained at a constant temperature of 25 °C on silver nitrate fluid mobilized within a range of 5 to 20 min. Glucose standard measurements were taken at 100 mg/dL in artificial urine. The observation results as shown in Fig. 11 indicate that longer drying times result in darker color boundaries. Analysis of the blue spectrum slope intensities was conducted for each color propagation formed, as depicted in Fig. 11. The analysis graph results indicate that blue intensity increases continuously up to 15 min and begins to decline at 20 min. Excessive dryness of the silver nitrate reagent in the detection zone can hinder the optimal formation of AgNPs. This is attributed to the loss of chemical activity of the silver nitrate reagent due to low humidity. Overly dry silver nitrate reagent in the detection zone can partially lose its chemical activity [34]. As illustrated in Fig. 11, a reagent drying time of 20 min results in the fading of the reaction diffusion boundaries. The low humidity at 20 min indicates reaction inhibition and a decrease in the signal intensity detected by ImageJ, as evidenced by the downward trend in the ImageJ graph at 20 min. This suggests the optimal drying time for the silver nitrate precursor solution is 15 min for reduction with 100 mg/dL glucose. Conversely, excessive drying time reduces the color characteristics of AgNP propagation, leading to darker color boundaries.

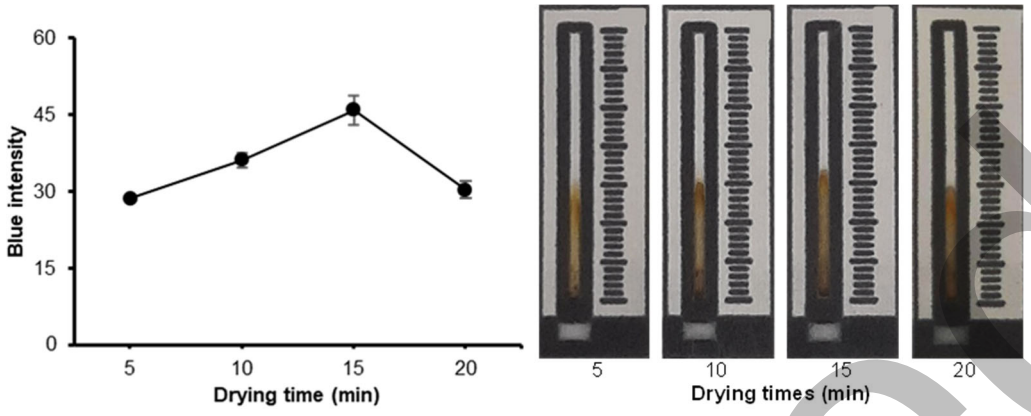

Fig 11. Effect of silver nitrate drying time on the detection zone of 3D-μPADs

The Influence of Immobilization Reagents

The effect of silver nitrate distribution on the detection zone of 3D-μPADs was studied through three variations of immobilization reagent observation. In the single immobilization, a single drop of silver nitrate solution was dispensed from bottom to top without any division. The double immobilization involved two drops dispensed in the same manner. Similarly, the triple immobilization utilized three drops. These variations are expected to offer insights into the relationship between silver nitrate distribution and reaction distance formation. The observation results indicate that the more immobilization performed, the fainter the color formed in the detection zone, as shown in Fig. 12. The analysis of the blue intensity slope shows that the more variations in the immobilization of silver nitrate fluid on the detection zone will decrease the slope value of the graph, as shown in graph Fig. 12. The downward trend in the graph indicates the fading of the observable color boundaries. This is clearly evident from both ImageJ readings and naked eye observation. Therefore, single-step reagent immobilization is considered the optimal silver nitrate distribution compared to multiple immobilization steps. This phenomenon shows that the distribution of the fluid precursor affects the formation of the optimal color boundary. The fluid distribution also affects the different drying times for each distribution in the detection zone. The fragmented drying time can result in a less optimal color boundary of the formed AgNPs.

Effect of Reaction Time

Reaction time is one of the important external factors that can control the quality of nanoparticle formation in addition to conditions such as temperature, pH, and pressure in the formation of AgNPs [35-37]. This phenomenon is also related to the assessment of NaOH's ability to accelerate the glucose oxidation process.

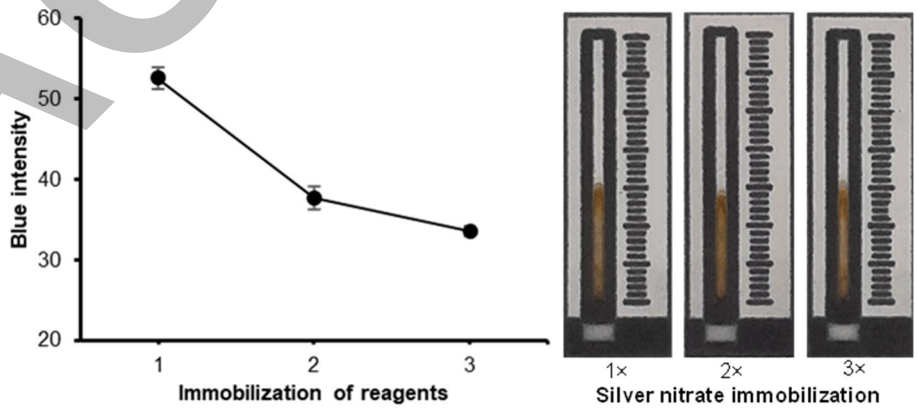

Fig 12. Effect of silver nitrate immobilization on the detection zone of 3D-μPADs

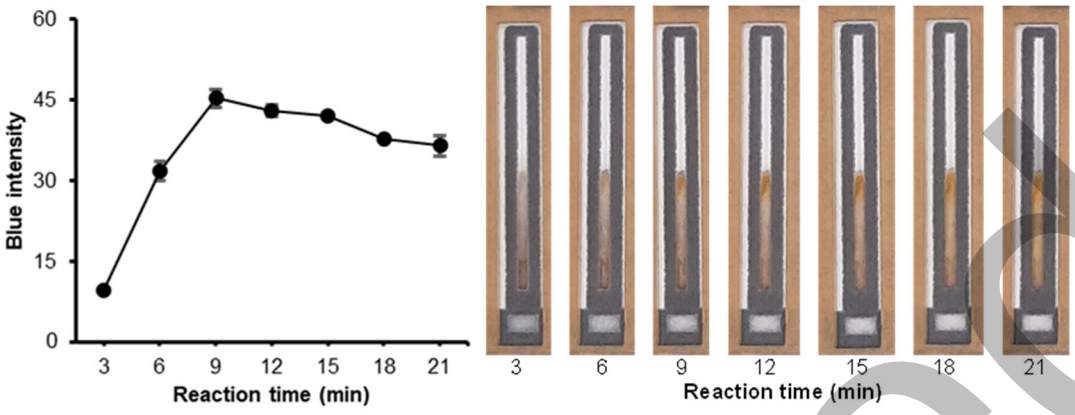

Fig 13. Effect of reaction time for the AgNPs formation on 3D-μPADs detection zone

In this detection method, the reaction time was observed at 3-min intervals. The observation results showed that the color boundary was clearly visible in some cases. However, color fading could be observed at longer times, as shown in Fig. 13. Direct light exposure to AgNP products can trigger their decomposition. This is attributed to the influence of light on the color formation of AgNPs. Despite the insignificant color change, decomposition can occur gradually. This condition is consistent with the trends observed in the graph. The blue intensity slope analysis showed that the optimal reaction time was obtained at 9 min with the next time showing a decreasing trend on the graph, as shown in Fig. 13. This phenomenon shows that the longer the reaction time for AgNPs, the more AgNPs are decomposed by light. This is attributed to the separation process that occurs between agglomerates and the solvent during the reaction time. This separation occurs due to the interaction between valence electrons and light radiation during exposure to light for a specific duration. The decomposition process causes the aggregates to break down and separate from the solvent if the reaction time is too long. Therefore, controlling the reaction time is crucial to prevent unwanted aggregation and maintain the quality of the final product. Excessively long reaction times can cause the aggregates to break down into undesirable forms. At the same time, excessively short reaction times are related to the kinetic influence of the reaction proceeding too quickly [38].

Validation Method

The optimal results from the previous optimization were applied to the linear analyte range of 0–100 mg/dL. Linearity is expected to prove the correlation phenomenon between the glucose analyte concentrate ion (x-axis) in artificial urine and the color reaction distance (y-axis) as the measurement calibration curve. Observations of glucose analyte variations were based on the x2-axis of the blue intensity spectrum using ImageJ. In addition, naked eye observation comparisons were also performed to review the reading results. Naked eye observation is performed by aligning the reaction distance to the 1 mm scale line that has been created on the right side of the 3D-μPADs design. The correlation between the two axes is expected to be in line with the reduced number of Ag^+ ions in the standard artificial urine solvent. The calibration curve results for the analyte range of 0–100 mg/dL are shown in Fig. 14(a). A comparison of the two measurements indicates that ImageJ analysis provides good results with a lower error rate compared to naked eye measurement. This is in line with the coefficient of determination (R^2) value from ImageJ analysis, which was obtained at 0.9905, higher than the naked eye measurement at 0.9808.

A precision test was conducted to review the repetition of measurements six times. This test aims to observe the measurement capability of 3D-μPADs under consistent conditions and influences [39]. Glucose measurement in artificial urine at 100 mg/dL showed some inconsistencies in two out of six readings. Six repeated tests showed that two data from six measurements differed by about 1 mm, as illustrated in Fig. 14(b). The precision test results showed that the %RSD of naked eye observation was 2.92% lower than the

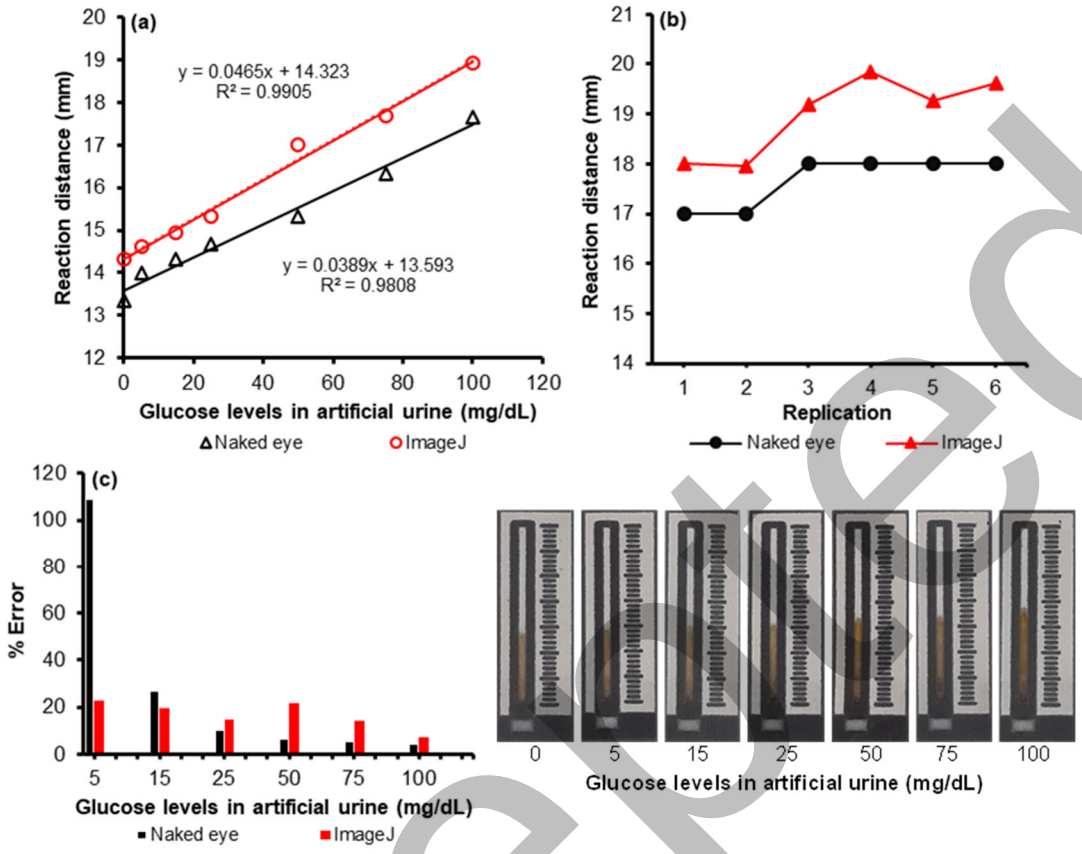

Fig 14. (a) Calibration curve, (b) precision test, and (c) %error rate of glucose measurement on 3D-μPADs

observation of ImageJ x2-axis measurement with %RSD of 4.27% (Table S3).

Accuracy testing was conducted to measure the proximity of glucose analyte readings to the actual value. This test was carried out on six glucose analyte samples in artificial urine ranging from 5 to 100 mg/dL. In Fig. 14(c), both the naked eye and ImageJ objective readings indicate that measurements are more accurate for high concentrations but less accurate for low concentrations. Specifically, ImageJ readings offer effective and flexible measurements across both high and low concentrations, although occasionally fluctuating. Conversely, naked eye objective readings demonstrate consistent accuracy for high concentrations but lower accuracy for low concentrations. The accuracy level of ImageJ readings is (77.32–92.58%), while naked eye objective readings reach (−9.25–95.28%). A detailed comparison of these methods is available in Table 2.

Table 2. Measurement results of glucose in artificial urine samples

Glucose level in urine artificial (mg/dL)	Reaction distance (n = 3)		Measured concentration (mg/dL)	
	Naked eye	ImageJ	Naked eye	ImageJ
5	14.0 ± 0.0	14.61 ± 0.21	10.5 ± 0.0 (109.3%)	6.13 ± 4.50 (22.68%)
15	14.3 ± 0.6	15.16 ± 1.06	19.0 ± 14.8 (26.9%)	17.93 ± 22.83 (19.55%)
25	14.7 ± 0.6	15.66 ± 0.88	27.6 ± 14.8 (10.4%)	28.69 ± 18.90 (14.76%)
50	15.7 ± 0.6	17.15 ± 0.57	53.3 ± 14.8 (6.6%)	60.72 ± 12.23 (21.44%)
75	16.7 ± 0.6	18.30 ± 0.37	79.0 ± 14.8 (5.4%)	85.45 ± 8.02 (13.93%)
100	17.7 ± 0.6	19.32 ± 0.82	104.7 ± 14.8 (4.7%)	107.42 ± 17.73 (7.42%)

*Number in parentheses under measured concentration represent the error of measurement. Measured concentration was calculated according to the calibration curve in Fig. 14(a)

In addition to the three previous method validations, the capability of 3D-μPADs to quantify analytes at the lowest concentration limits is an important aspect that needs to be reviewed. This capability demonstrates that the 3D-μPADs measurement method can provide accurate results at deficient analyte concentrations. Further analysis shows that the sensitivity of ImageJ measurements is better than that of naked eye observation. The LOD value using ImageJ is 11.11 mg/dL, while the LOD value with naked eye observation is 14.79 mg/dL. These results indicate that ImageJ-based measurements are superior to naked eye-based measurements.

Following method validation, the 3D-μPADs measurement method was successfully developed as a glucose level analysis method in artificial urine, generating accurate, precise, and reliable data. This development resulted in a measurement method with high portability, low fabrication costs, and minimal sample requirements. However, a limitation encountered during this method's development is the sensitivity issue, which requires further evaluation. This sensitivity issue is evident in the standard curve, which shows insignificant differences in reaction distance between analyte concentrations, typically around ≤ 1 mm (Fig. 14(b)). Such small differences in reaction length can lead to measurement errors. While other methods like electrochemistry, spectrophotometry, or fluorescence can better address sensitivity issues, the 3D-μPADs method cannot be overlooked [40]. If further development can successfully improve this sensitivity issue, the 3D-μPADs method could become superior to other methods. Moreover, not all regions have access to advanced measurement technologies such as laboratory instruments. Therefore, further development of 3D-μPADs presents an alternative that can meet the needs of body glucose level monitoring.

■ CONCLUSION

A new alternative method for early diagnosis of glucose levels has been successfully developed through a non-enzymatic synthesis of AgNPs on 3D-μPADs. This detection system is improved by incorporating a 3D connector that can directly limit the mixing of reagents between the sample and detection zones. The optimum conditions obtained include the determination of the reaction procedure as follows: detection zone containing 30 mM $AgNO_3$ and sample zone consisting of the mixture of glucose in artificial urine, 10 M NaOH 10 M, and 1% starch. Additionally, the method needs only a single immobilization of the reagent and a detection time of 9 min. Good linearity (R^2 = 0.9905), excellent precision (%RSD = 4.27%), accuracy (77.32–92.58%), and LOD (11.11 mg/dL) could be attributed to the developed 3D-μPADs. Upon successful development, the glucose measurement method using 3D-μPADs presents several advantages, including high portability, low fabrication costs, and minimal sample requirements. However, the method exhibits limitations in measurement sensitivity compared to other established methods. Despite these limitations, the potential of this method cannot be overlooked due to its high portability. This allows many areas with limited healthcare access to monitor body glucose levels without worry.

■ ACKNOWLEDGMENTS

We would like to thank the Institute of Research and Community Services Brawijaya University (LPMM) from Brawijaya University for the financial support through the 2024 Research Ecosystem Strengthening Grant (No.00144.10/UN10.A0501/B/PT.01.03.2/2024).

■ CONFLICT OF INTEREST

The authors have no conflict of interest.

■ AUTHOR CONTRIBUTIONS

Ahmad Luthfi Fahmi conducted experiments and data analysis, wrote the original manuscript, and revised the manuscript. Kamila Rohadatul 'Aisy assisted in writing the original manuscript and revising the manuscript. Ika Oktavia Wulandari conceptualized the idea, supervised the project, and revised the manuscript. Hermin Sulistyarti conceptualized the idea, supervised the project, and revised the manuscript. Akhmad Sabarudin conceptualized the idea, provided funding, supervised the project, and revised the manuscript.

■ REFERENCES

[1] Farmaki, P., Damaskos, C., Garmpis, N., Garmpi, A., Savvanis, S., and Diamantis, E., 2021, Complications of the type 2 diabetes mellitus, *Curr. Cardiol. Rev.*, 16 (4), 249–251.

[2] Tomic, D., Shaw, J.E., and Magliano, D.J., 2022, The burden and risks of emerging complications of diabetes mellitus, *Nat. Rev. Endocrinol.*, 18 (9), 525–539.

[3] Elhefnawy, M.E., Sheikh Ghadzi, S.M., and Noor Harun, S., 2022, Predictors associated with type 2 diabetes mellitus complications over time: A literature review, *J. Vasc. Dis.*, 1 (1), 13–23.

[4] Qaid, M.M., and Abdelrahman, M.M., 2016, Role of insulin and other related hormones in energy metabolism—A review, *Cogent Food Agric.*, 2 (1), 1267691.

[5] Zhao, X., An, X., Yang, C., Sun, W., Ji, H., and Lian, F., 2023, The crucial role and mechanism of insulin resistance in metabolic disease, *Front. Endocrinol.*, 14, 1149239.

[6] Rahman, M.S., Hossain, K.S., Das, S., Kundu, S., Adegoke, E.O., Rahman, M.A., Hannan, M.A., Uddin, M.J., and Pang, M.G., 2021, Role of insulin in health and disease: An update, *Int. J. Mol. Sci.*, 22 (12), 6403.

[7] Galicia-Garcia, U., Benito-Vicente, A., Jebari, S., Larrea-Sebal, A., Siddiqi, H., Uribe, K.B., Ostolaza, H., and Martín, C., 2020, Pathophysiology of type 2 diabetes mellitus, *Int. J. Mol. Sci.*, 21 (17), 6275.

[8] Mng'agi, M.O., Mwandigha, A.M., and Mbugi, E.V., 2023, Gender-inclined young age glycosuria: Contribution to late age chronic renal diseases, type 2 diabetes mellitus and cardiovascular diseases, *East Afr. Health Res. J.*, 7 (1), 88–93.

[9] Vargas-Delgado, A.P., Arteaga Herrera, E., Tumbaco Mite, C., Delgado Cedeno, P., Van Loon, M.C., and Badimon, J.J., 2023, Renal and cardiovascular metabolic impact caused by ketogenesis of the SGLT2 inhibitors, *Int. J. Mol. Sci.*, 24 (4), 4144.

[10] Tuttle, K.R., 2017, Back to the future: Glomerular hyperfiltration and the diabetic kidney, *Diabetes*, 66 (1), 14–16.

[11] Prapaporn, S., Arisara, S., Wunpen, C., and Wijitar, D., 2020, Nanocellulose films to improve the performance of distance-based glucose detection in paper-based microfluidic devices, *Anal. Sci.*, 36 (12), 1447–1451.

[12] Jalil, A.T., Ashfaq, S., Bokov, D., Alanazi, A., Hachem, K., Suksatan, W., and Sillanpää, M., 2021, High-sensitivity biosensor based on glass resonance PhC cavities for detection of blood component and glucose concentration in human urine, *Coatings*, 11 (12), 1555.

[13] Hemmati, S., Retzlaff-Roberts, E., Scott, C., and Harris, M.T., 2019, Artificial sweeteners and sugar ingredients as reducing agent for green synthesis of silver nanoparticles, *J. Nanomater.*, 2019 (1), 9641860.

[14] Pascu, B., Negrea, A., Ciopec, M., Duteanu, N., Negrea, P., Nemeş, N.S., Seiman, C., Marian, E., and Micle, O., 2021, A green, simple and facile way to synthesize silver nanoparticles using soluble starch. pH studies and antimicrobial applications, *Materials*, 14 (16), 4765.

[15] Swensson, B., Ek, M., and Gray, D.G., 2018, In situ preparation of silver nanoparticles in paper by reduction with alkaline glucose solutions, *ACS Omega*, 3 (8), 9449–9452.

[16] Durmazel, S., Üzer, A., Erbil, B., Sayın, B., and Apak, R., 2019, Silver nanoparticle formation-based colorimetric determination of reducing sugars in food extracts via Tollens' reagent, *ACS Omega*, 4 (4), 7596–7604.

[17] Chen, Z., Wright, C., Dincel, O., Chi, T.Y., and Kameoka, J., 2020, A low-cost paper glucose sensor with molecularly imprinted polyaniline electrode, *Sensors*, 20 (4), 1098.

[18] Nishat, S., Jafry, A.T., Martinez, A.W., and Awan, F.R., 2021, Paper-based microfluidics: Simplified fabrication and assay methods, *Sens. Actuators, B*, 336, 129681.

[19] Nguyen, H.Q., Nguyen, V.D., Phan, V.M., and Seo, T.S., 2024, A novel point-of-care platform for rapid SARS-CoV-2 detection utilizing an all-in-one 3D-

printed microfluidic cartridge and IoT technology, *Sens. Actuators, B*, 410, 135632.

[20] Gerold, C.T., Bakker, E., and Henry, C.S., 2018, Selective distance-based K^+ quantification on paper-based microfluidics, *Anal. Chem.*, 90 (7), 4894–4900.

[21] Al-Jaf, S.H., and Omer, K.M., 2022, Enhancing of detection resolution via designing of a multi-functional 3D connector between sampling and detection zones in distance-based microfluidic paper-based analytical device: Multi-channel design for multiplex analysis, *Microchim. Acta*, 189 (12), 482.

[22] Altundemir, S., Uguz, A.K., and Ulgen, K., 2017, A review on wax printed microfluidic paper-based devices for international health, *Biomicrofluidics*, 11 (4), 041501.

[23] Hiraoka, R., Kuwahara, K., Wen, Y.C., Yen, T.H., Hiruta, Y., Cheng, C.M., and Citterio, D., 2020, Paper-based device for naked eye urinary albumin/creatinine ratio evaluation, *ACS Sens.*, 5 (4), 1110–1118.

[24] Kumar, S.V., Bafana, A.P., Pawar, P., Rahman, A., Dahoumane, S.A., and Jeffryes, C.S., 2018, High conversion synthesis of <10 nm starch-stabilized silver nanoparticles using microwave technology, *Sci. Rep.*, 8 (1), 5106.

[25] Salaheldin, H.I., 2018, Corrigendum: Optimizing the synthesis conditions of silver nanoparticles using corn starch and their catalytic reduction of 4-nitrophenol (*Adv. Nat. Sci: Nanosci. Nanotechnol.* 9 025013), *Adv. Nat. Sci: Nanosci. Nanotechnol.*, 9 (3), 039501.

[26] Jung, J., Raghavendra, G.M., Kim, D., and Seo, J., 2018, One-step synthesis of starch-silver nanoparticle solution and its application to antibacterial paper coating, *Int. J. Biol. Macromol.*, 107, 2285–2290.

[27] El-Rafie, M.H., Ahmed, H.B., and Zahran, M.K., 2014, Facile precursor for synthesis of silver nanoparticles using alkali treated maize starch, *Int. Scholarly Res. Not.*, 2014 (1), 702396.

[28] Nguyen, H.T., Nguyen, T.D., Nguyen, D.P., Thai, N.T.T., and Nguyen, T.H., 2022, Synthesis efficiency of silver nanoparticles by light-emitting diode and microwave irradiation using starch as a reducing agent, *Nanotechnol. Environ. Eng.*, 7 (1), 297–306.

[29] Ponsanti, K., Tangnorawich, B., Ngernyuang, N., and Pechyen, C., 2020, A flower shape-green synthesis and characterization of silver nanoparticles (AgNPs) with different starch as a reducing agent, *J. Mater. Res. Technol.*, 9 (5), 11003–11012.

[30] Jiang, S., Xing, X., Wang, L., Yang, S., Xiao, J., Zhang, Q., Xu, X., Peng, M., and Wang, X., 2021, Insight into the effect of pH-adjusted acid on thermodynamic properties and crystallization sequence during evaporative-crystallization process of hydrolyzed urine, *Environ. Sci. Pollut. Res.*, 28 (22), 28507–28517.

[31] Soda, Y., Robinson, K.J., Cherubini, T.J., and Bakker, E., 2020, Colorimetric absorbance mapping and quantitation on paper-based analytical devices, *Lab Chip*, 20 (8), 1441–1448.

[32] Xing, R., Jiao, T., Zhou, J., Zhang, Q., and Peng, Q., 2016, Preparation and photocatalytic property of silver nanoparticles using cationic pyridine derivative, *Integr. Ferroelectr.*, 169 (1), 15–21.

[33] Hill, Jr., R.H., and Finster, D.C., 2016, *Laboratory Safety for Chemistry Students*, John Wiley & Sons Inc., New York, US.

[34] Apyari, V.V., Furletov, A.A., Garshev, A.V., Volkov, P.A., Gorbunova, M.O., and Shevchenko, A.V., 2017, Preparation of reagent indicator papers with silver triangular nanoplates for chemical analysis, *Moscow Univ. Chem. Bull.*, 72 (4), 167–173.

[35] Dankovich, T.A., 2014, Microwave-assisted incorporation of silver nanoparticles in paper for point-of-use water purification, *Environ. Sci.: Nano*, 1 (4), 367–378.

[36] Patra, J.K., and Baek, K.H., 2014, Green nanobiotechnology: Factors affecting synthesis and characterization techniques, *J. Nanomater.*, 2014 (1), 417305.

[37] Yaqoob, A.A., Umar, K., and Ibrahim, M.N.M., 2020, Silver nanoparticles: Various methods of synthesis, size affecting factors and their potential

applications–A review, *Appl. Nanosci.*, 10 (5), 1369–1378.

[38] Trieu, Q.A., Le, C.T.B., Pham, C.M., and Bui, T.H., 2023, Photocatalytic degradation of methylene blue and antibacterial activity of silver nanoparticles synthesized from *Camellia sinensis* leaf extract, *J. Exp. Nanosci.*, 18 (1), 2225759.

[39] Zanobini, A., Sereni, B., Catelani, M., and Ciani, L., 2016, Repeatability and Reproducibility techniques for the analysis of measurement systems, *Measurement*, 86, 125–132.

[40] Tang, L., Chang, S.J., Chen, C.J., and Liu, J.T., 2020, Non-invasive blood glucose monitoring technology: A review, *Sensors*, 20 (23), 6925.